Multicarrier enabled Baseband Subsampling MIMO System (MBS-MIMO)

Franz G. Aletsee and Reinhard Stolle
Augsburg University of Applied Sciences
Augsburg, Germany
franz.aletsee@hs-augsburg.de

***Abstract*—Due to the growing demand for higher bitrates, modern communication systems require more and more analog bandwidth or, alternatively, spectral efficiency. With increasing sampling frequencies, analog-to-digital converters (ADC) suffer from a decrease in the effective number of bits (ENOB) [1]. For wired communication systems, where quantization noise is often the predominant limitation of the signal-to-noise ratio (SNR), it is desired to have a high ENOB in combination with a high analog bandwidth. A state-of-the-art solution are interleaving ADCs which, however, come with various challenges like gain, phase, and DC offsets that result in a decreased SNR. This paper presents a technique that utilizes the advantages of interleaving ADCs but avoids most of their disadvantages. It is based on filterbank subsampling and allows a high degree of parallelization. Through the use of discrete multitone (DMT) modulation, even high amounts of alias can be treated the same way as crosstalk in a multiple-input multiple-output (MIMO) system. The paper presents the theoretical background of the system and its verification by simulations as well as measurements with an experimental system.**

***Index Terms*—multicarrier, subsampling, filterbank, MIMO, MBS-MIMO**

I. Introduction

To further increase the data rates, both a large analog bandwidth and a high ADC resolution are required. Choosing an ADC is always a tradeoff between resolution and analog bandwidth [1], [2]. In Sec. I we will motivate and propose a DMT based subsampling system which is theoretically described in Sec. II. In Sec. III and IV we will show a time domain simulation of the system to verify the proposed idea. Finally, in Sec. V we present measurement results from an experimental setup.

A. Time Interleaving ADCs

Interleaving ADCs provide a possible solution by employing the analog signal to several ADCs in parallel. Those ADCs need to be configured in a way that they sample the same analog signal at a fixed phase relation to each other. Unfortunately, they suffer from mismatch errors among each other like offset mismatch (OM), gain mismatch (GM), and timing skew mismatch (TM) [3]. Any mismatch results in signal degradation and a reduced dynamic range [4].

This work was supported by Rosenberger Hochfrequenztechnik GmbH.

B. Nyquist Band Separation

Theoretically, the best solution would be to subdivide the analog signal into N subbands with perfectly rectangularly shaped filters. All subbands could be sampled independently by an individual ADC satisfying Nyquist's theorem. This approach would have the advantage the subbands being available as separate streams and the ADCs sample in parallel. In addition, the voltage level at all ADCs would be reduced due to the fact that only a fraction of the signal power is directed to each of them. This could increases the SNR, since quantization noise is decreased.

C. Hybrid Filter Banks

As rectangularly shaped filters are technically not realizable, filterbanks with sharp edges have been used [5]. Even in this case, due to the finite attenuation of frequencies outside the Nyquist zone, alias occurs. This alias degrades the signal quality and reduces channel capacity. To remove the impact of alias, hybrid filter banks have been proposed [6], [7]. Such a system is shown in Fig. 1. They combine the samples of the different ADCs in a manner that alias is removed in the digital domain. As a result, the Nyquist band is available for further processing.

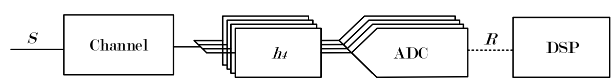

Fig. 1: System model with $M = 4$ ADCs sampling in parallel, each preceded by an analog filter.

II. Theory of a DMT enabled Baseband Subsampling System

A. Mathematical Description of Multicarrier enabled Baseband Subsampling MIMO (MBS-MIMO)

A typical DMT signal [8] is composed of $k = -K...K$ carriers that are spaced by Δf and orthogonal to one another. Each carrier contains a stream of complex symbols in the IQ plane which carries the desired information content. Such a DMT signal is shown in Fig. 2(a) with one exemplary carrier in each Nyquist band of the respective receiving ADC.

Sampling such a signal with an ADC whose sample rate f_s is an integer multiple of the signal's carrier spacing, preserves the carrier's orthogonality. Equation (1) describes mathematically the effect of filtering (F_m) and subsampling an analog DMT signal with unrestricted bandwidth.

$$R_m(k\Delta f) = \sum_{l=-\infty}^{+\infty} F_m(k\Delta f - lf_s) \cdot S(k\Delta f - lf_s) \quad (1)$$

A superposition of carriers in the baseband can be observed. The result can be seen with the exemplary carriers in Fig. 2(b).

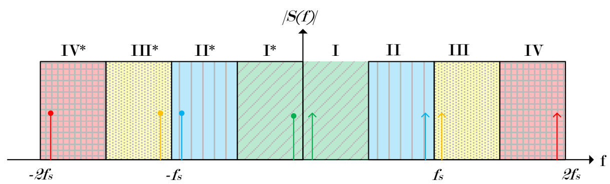

(a) The transmitted DMT signal (S) with four Nyquist zones and four exemplary carriers.

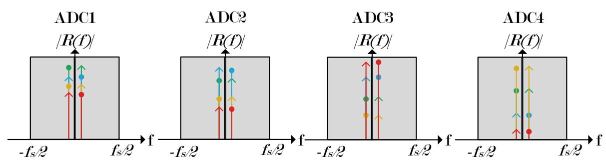

(b) The subsampled and filtered DMT signal at each ADC that contains the filtered superposition of the transmitted signal.

Fig. 2: DMT signal before and after subsampling.

If the transmitted DMT signal (S_1) consists of N Nyquist bands, a minimum of $M = N$ ADCs are required. As a consequence the signal (S_1) contains $N \cdot K$ carriers. In order to describe the system in a more convenient way, several steps need to be done. A baseband transformation can be applied to the transmitted signal as (2) shows.

$$S_I^{BB}(k\Delta f) = \begin{bmatrix} S_1(f_1) \\ S_1(f_2)^* \\ \vdots \\ S_1(f_N) \end{bmatrix} \quad (2)$$

This is accomplished by transforming each orthogonal carrier k to its corresponding baseband frequency using (3). One should note, that each even Nyquist band needs to be complex conjugated since the DMT signal is real valued. The complex conjugate is denoted by ($*$). The index of (S_I^{BB}) means, that this signal is the first DMT signal which will be needed in subsection B.

$$f_n(k\Delta f) = \begin{cases} \frac{n-1}{2} \cdot fs + k\Delta f & \text{if } n \text{ is odd,} \\ \frac{n}{2} \cdot fs - k\Delta f & \text{if } n \text{ is even} \end{cases} \quad (3)$$

The same can be done with the analog filters. Equation (4) shows the baseband representation of these filters where the m-th row of the matrix contains the complex filter transfer functions at the corresponding Nyquist band n. The associated frequencies can also be taken from (3). As it is true for the transmitted signal, transfer functions from even Nyquist bands have to be complex conjugated since they represent real systems.

$$\mathbf{F}(k\Delta f) = \begin{bmatrix} F_1(f_1) & F_1(f_2)^* & \cdots & F_1(f_N) \\ \vdots & \vdots & \ddots & \vdots \\ F_M(f_1) & F_M(f_2)^* & \cdots & F_M(f_N) \end{bmatrix} \quad (4)$$

If one would like to incorporate a transmission channel, it must also be transformed to its baseband representation as (5) shows.

$$\mathbf{C}(k\Delta f) = \begin{bmatrix} C(f_1) & 0 & 0 \\ 0 & C(f_2)^* & 0 \\ \vdots & \ddots & \vdots \\ 0 & \cdots & C(f_N) \end{bmatrix} \quad (5)$$

The baseband channel matrix $\mathbf{C}$ is a diagonal matrix with the channel transfer function on its main diagonal. To describe the cascade of the channel and the analog filters, both matrices must be multiplied as shown in (6).

$$\mathbf{H}(k\Delta f) = \mathbf{F}(k\Delta f) \cdot \mathbf{C}(k\Delta f) \quad (6)$$

$$R_I(k\Delta f) = \begin{bmatrix} R_1(k\Delta f) \\ R_2(k\Delta f) \\ \vdots \\ R_M(k\Delta f) \end{bmatrix} \quad (7)$$

The M ADCs provide the subsampled DMT signal, which can be grouped together in a vector as (7) shows.

$$R_I(k\Delta f) = \mathbf{H}(k\Delta f) \cdot S_I^{BB}(k\Delta f) \quad (8)$$

Finally, the linear equation (1) can be compactly written in baseband representation (8) for all M filtered baseband signals (7) using vector notation. Fig. 3 graphically illustrates (8).

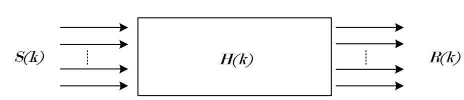

Fig. 3: Alias in subsampling systems can be seen the same way as multi-path propagation in MIMO systems.

The system described above is perfectly equivalent to the model of MIMO systems, except that the different propagation paths originate from filtering and subsampling. Therefore, known MIMO techniques can directly be applied to MBS-MIMO.

B. Model Extension to Multiple Channels

In the previous section only one DMT signal (S_I^{BB}) consisting of N Nyquist bands was considered. A higher datarate can be achieved with MBS-MIMO when operating several channels in parallel. This can be integrated into the formalism by aggregating the baseband signals of the distinct channels as shown in (9).

$$S^{BB}(k\Delta f) = \begin{bmatrix} S_I^{BB} \\ S_{II}^{BB} \\ \vdots \\ S_P^{BB} \end{bmatrix} = \begin{bmatrix} S_1(f_1) \\ S_1^*(f_2) \\ \vdots \\ S_2(f_1) \\ S_2^*(f_2) \\ \vdots \end{bmatrix} \tag{9}$$

The channel matrix $\mathbf{C}$ has to be extended in a similar fashion and crosstalk between the channels has to be included, resulting in

$$\mathbf{C}(k\Delta f) = \begin{bmatrix} \mathbf{T}_{I,I} & \mathbf{X}_{I,II} & \cdots & \mathbf{X}_{I,P} \\ \mathbf{X}_{II,I} & \mathbf{T}_{II,II} & \cdots & \mathbf{X}_{II,P} \\ \vdots & \vdots & \ddots & \vdots \\ \mathbf{X}_{P,I} & \mathbf{X}_{P,II} & \cdots & \mathbf{T}_{PP} \end{bmatrix} \tag{10}$$

Each matrix element in (10) is a matrix itself, which is given by (5). The arguments of the matrix elements ($k\Delta f$) have been omitted.

$$\mathbf{F}(k\Delta f) = \begin{bmatrix} \mathbf{F}_I & 0 & \cdots & 0 \\ 0 & \mathbf{F}_{II} & \cdots & 0 \\ \vdots & \vdots & \ddots & \vdots \\ 0 & 0 & \cdots & \mathbf{F}_P \end{bmatrix} \tag{11}$$

The same needs to be done with the filter matrix $\mathbf{F}$ as (11) shows. Each diagonal element in (11) is a complex $M \times M$ matrix containing the filter transfer functions of the P sets of M analog filters according to (4).

$$R(k\Delta f) = \begin{bmatrix} R_I(k\Delta f) \\ R_{II}(k\Delta f) \\ \vdots \\ R_P(k\Delta f) \end{bmatrix} \tag{12}$$

Each vector element in (12) contains $M \cdot P$ entries that describe superimposed carriers from different Nyquist bands and the result of crosstalk.

$$R(k\Delta f) = \mathbf{F}(k\Delta f) \cdot \mathbf{C}(k\Delta f) \cdot S^{BB}(k\Delta f) \tag{13}$$

Finally, the system can be described with the linear equation shown in (13). It does not make any difference for the system, whether alias or crosstalk is the cause of the superposition of carriers. Therefore, they can be treated equivalently.

C. Equalization of a DMT Signal

For each baseband carrier, a matrix $\mathbf{W}$ needs to be calculated to estimate the transmitted signal ($\widehat{S}^{BB}$) correctly, cf. (14).

$$\widehat{S}^{BB}(k\Delta f) = \mathbf{W}(k\Delta f) \cdot R(k\Delta f) \tag{14}$$

This can be done for example by Zero Forcing, i.e. via inverting the matrix $\mathbf{H}$. This is not the optimal solution in regard to noise present in the system. The performance of symbol recovery highly depends on how the matrix $\mathbf{W}$ is conditioned. Hence, we call the matrices $\mathbf{W}$ equalizer matrices.

D. Sample Clock Considerations

One major advantage of the MBS-MIMO approach is that the ADCs do not need an exact phase relation to each other. Phase or delay locked loops for phase adjustments can be omitted. The sampling clock does not need to be synchronous. Coherency is sufficient, which means the phase relation between ADCs can be arbitrary but must be time invariant. In consequence, no length matching is required. In fact, since the phase relations between the ADCs are incorporated in the equalizer matrices $\mathbf{W}$, slow changes in the phase relations can be permitted without compromising the system. In this context, slow is to be understood in relation to the symbol rate of the DMT signal. Consequently, slow thermal drifts can be tracked. The equalizer matrix can be adapted to perform decision directed equalization, for instance. Since subsampling is highly susceptible to jitter, a low phase noise sampling source is mandatory. However, the same requirements apply just as well to time interleaved ADCs.

E. Advantages of MBS-MIMO

MBS-MIMO has several advantages over time interleaved sampling. Gain mismatch (GM) and timing mismatch (TM) do not need to be corrected, as this is done intrinsically by the equalizer. In addition, quantization noise is reduced due to the input signal being filtered before sampling which reduces the drive of all ADCs, while in time interleaved sampling all ADCs encounter the full signal amplitude. Since the DMT carriers are orthogonal to each other and the sample rate of the ADCs is an integer fraction of the analog bandwidth, the equalizer can be highly parallelized. DMT systems have proven to perform well under various noise conditions [9]–[11]. Furthermore, in theory the system is scalable since more analog bandwidth can be exploited by adding more ADCs and only limited by the channel bandwidth. Low jitter clocks and a large analog bandwidth are the main cost factors.

III. Simulation Setup

To prove the functionality of the system, a MATLAB based time domain simulation was carried out. Figure 4 shows the schematic of the simulation model consisting of a cable model with two coupled channels and 4 subbands each at the receiver.

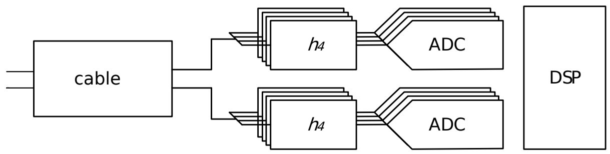

Fig. 4: A two channel four subband model is used to verify the concept with a MATLAB simulation.

A. ADC Model

The eight ADCs in total are modeled as uniform quantizers with a resolution of 10 bits followed by a saturation block. The ADCs sample coherently at 100 MHz and are preceded by an individually configurable programmable gain amplifier (PGA). Each PGA is tuned on the basis of a given crest factor (CF). Amplitudes exceeding the maximal quantization levels are clipped. Jitter is neglected in the model. The particular processing steps for one subband are illustrated in form of a schematic in Fig. 5.

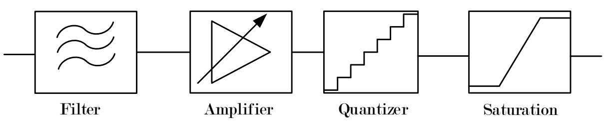

Fig. 5: The ADC is modeled as a uniform quantizer with saturation. A PGA adjusts the filtered input signal amplitude applied to the ADC.

B. Analog Frontend and Channel Model

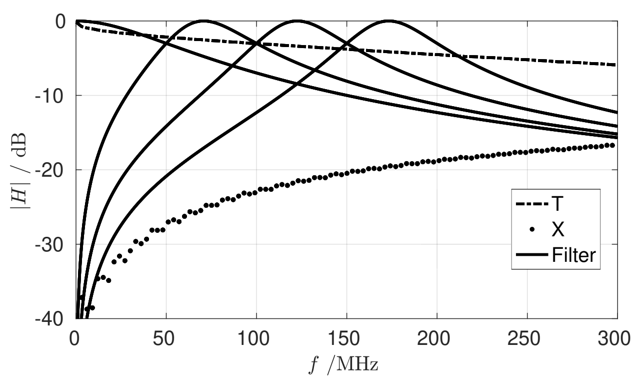

Fig. 6: Shown are transmission (T) and crosstalk (X) of a 15m Rosenberger HSD cable as used within the simulation. The analog frontend filters are first order butterworth filters with cutoff frequencies at the corresponding subband edges.

Figure 6 shows the filter transfer functions of the four analog filters modeled as first order butterworth filters. Their cut-off frequencies are designed to coincide with the subband boundaries. These filters have been chosen because of their poor roll-off which ensures enough alias to validate the concept. Figure 6 also provides the measured transmission and crosstalk of a 15m Rosenberger HSD cable. Two wires have been used in single-ended operation to achieve a high level of crosstalk at low frequencies. This was done to verify the MIMO capabilities of the system even at low frequencies, hence the spread between crosstalk and transmission at 200 MHz is as small as about 14 dB, see Fig. 6. The frontend filter bank, crosstalk and transmission are identical for both cable channels in the simulation.

C. Configuration of the DMT Signal

The DMT signal is generated completely within MATLAB. The simulation does not use a DAC model. All essential parameters can be looked up in Tab. I. The constellation size on each carrier is chosen individually, based on the estimated SNR. All carriers except DC and the carriers that coincide with multiples of the Nyquist frequency are used.

TABLE I: Systemparameters of the DMT Signal

Parameter	Value
FFT Length (baseband)	512
F_{adc}	100 MHz
Δf	195 kHz
ENOB (ADC)	10 Bit
Cyclic Prefix length	10 samples
Crest Factor (CF)	5
BER (uncoded)	10^{-5}
Datarate @ 2x200 MHz	5.6 Gbit/s

D. Sample Rate Control and Symbol Detection

Since the goal of this paper was to prove the principle of MBS-MIMO, any timing or symbol offset between transmitter and receiver was neglected. In real systems, these can degrade system performance. However, sample rate control and symbol detection are state-of-the-art and are therefore omitted for this proof of concept. The first 50 symbols are assumed to be a known training sequence to initialize the equalizer matrix. The estimate is calculated by minimizing the mean square error of $\mathbf{W}$ for the training sequence.

IV. Simulation Results

A subset of the elements of the inverse equalizer matrices from all carriers are shown in Fig. 7. The SNR calculated for each carrier is shown in baseband representation in Fig. 8.

With this approach, a simplex data rate of 5.6 GBit/s has been predicted by simulation.

V. Experimental Verification

To verify the concept with actual hardware, a FPGA based prototype with signal replaying and recording capability has been built. The same system parameters as in the simulation have been used except for the analog filters and the PGAs of the ADCs. Those have been implemented to match the impedance of the cable which adds about 6 dB of attenuation at 200 MHz. In contrast to the simulation model the actual

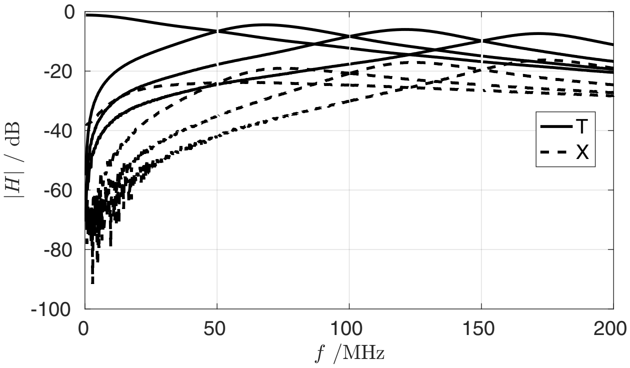

Fig. 7: The inverted equalizer matrix is an estimation of the transfer function of the channel at the respective carrier's frequency.

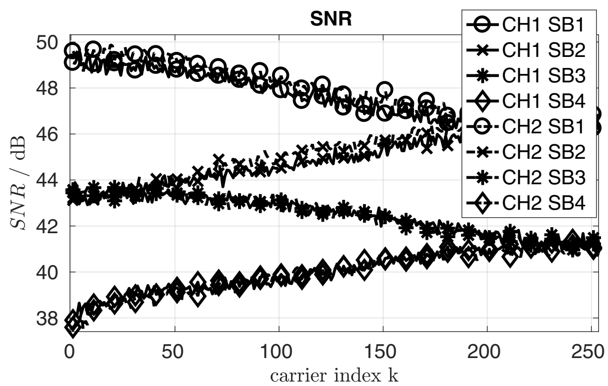

Fig. 8: The SNR for each carrier in both channels are shown in baseband representation.

PGAs are limited to a maximum gain of 12 dB. The start of the transmission is indicated by a trigger signal. Transmitter and receiver are clocked by the same reference oscillator allowing the proof of concept without the need to consider timing issues.

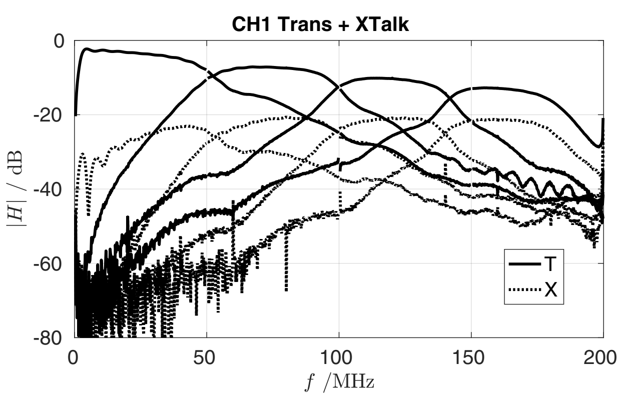

Fig. 9: Inverted equalizer matrix of the experimental setup.

Figure 9 shows the inverted equalizer matrix for both, transmission and crosstalk. For the experimental setup we predict a lower data rate of 2.07 GBits/s due to the reasons stated above. The predicted data rate was confirmed by transmitting 10000 symbols per carrier. The high pass characteristics of the transformers from the prototype boards can be observed. At 180 MHz crosstalk and transmission differ by less than 9 dB.

VI. Summary and Conclusion

When multiple DMT modulated signals are filtered and subsampled by ADCs, the resulting alias can be treated the same way as multi-channel propagation in MIMO systems, hence established techniques from MIMO systems can be applied directly. Since multiple ADCs provide their data in parallel and the carriers stay orthogonal under the described circumstances, signal processing can be highly parallelized. Moreover, it has been shown, that the concept also provides several advantages over timing interleaved ADCs.

VII. Outlook

To accurately predict the system performance without the hassle of running time consuming time domain simulations, a frequency domain model will be developed and compared to time domain simulations. The presented concept also applies for the transmitter side which will be presented in an upcoming publication.

References

[1] R. H. Walden, "Analog-to-digital converter survey and analysis," *IEEE Journal on Selected Areas in Communications*, vol. 17, no. 4, pp. 539–550, Apr. 1999.

[2] B. Murmann, "The race for the extra decibel: A brief review of current ADC performance trajectories," *IEEE Solid-State Circuits Magazine*, vol. 7, no. 3, pp. 58–66, 2015.

[3] A. Buchwald, "High-speed time interleaved adcs," *IEEE Communications Magazine*, vol. 54, no. 4, pp. 71–77, April 2016.

[4] A. Petraglia and S. K. Mitra, "Analysis of mismatch effects among A/D converters in a time-interleaved waveform digitizer," *IEEE Transactions on Instrumentation and Measurement*, vol. 40, no. 5, pp. 831–835, Oct. 1991.

[5] Z. Song, C. Lelandais-Perrault, and P. Bénabes, "Synthesis of complex subband hybrid filter banks A/D converters using adaptive filters," in *Proc. 16th IEEE Int. Conf. Electronics Circuits and Systems - (ICECS 2009)*, Dec. 2009, pp. 399–402.

[6] X. Liu, W. Li, J. Wei, and L. Cheng, "Adaptable hybrid filter bank analog-to-digital converters for simplifying wideband receivers," *IEEE Communications Letters*, vol. 21, no. 7, pp. 1525–1528, Jul. 2017.

[7] B. Szlachetko and O. Venard, "Hybrid filter bank design and analysis," in *Proc. and Applications (SPA) 2013 Signal Processing: Algorithms, Architectures, Arrangements*, Sep. 2013, pp. 129–132.

[8] J. A. C. Bingham, "Multicarrier modulation for data transmission: an idea whose time has come," *IEEE Communications Magazine*, vol. 28, no. 5, pp. 5–14, May 1990.

[9] M. Ghosh, "Analysis of the effect of impulse noise on multicarrier and single carrier QAM systems," *IEEE Transactions on Communications*, vol. 44, no. 2, pp. 145–147, Feb. 1996.

[10] M. Ouzzif, D. Toumpakaris, J. Cioffi, and A. Zeddam, "Comparison of QAM-VDSL and DMT-VDSL in an impulse noise environment," in *Proc. IEEE Global Telecommunications Conf. GLOBECOM '03*, vol. 4, Dec. 2003, pp. 2141–2145 vol.4.

[11] N. H. Nedev, S. McLaughlin, and D. I. Laurenson, "Estimating errors in transmission systems due to impulse noise," *IEE Proceedings-Communications*, vol. 153, no. 5, pp. 651–656, Oct. 2006.